2019 32nd International Conference on VLSI Design and 2019 18th International Conference on Embedded Systems (VLSID)

Insights on anisotropic dissipative quantum transport in n-type Phosphorene MOSFET

Madhuchhanda Brahma*†, Arnab Kabiraj†, Santanu Mahapatra†,
*Centre for NanoScience and Engineering, Indian Institute of Science, Bangalore, India
†Nanoscale Device Research Laboratory, Dept. of Electronic Systems Engineering, Indian Institute of Science, Bangalore, India
Email: madhuchhanda@iisc.ac.in, kabiraj@iisc.in, santanu@iisc.ac.in

***Abstract*—We study the quantum dissipative transport in Phosphorene n-type metal oxide semiconductor field effect transistor (MOSFET) in armchair and zigzag directions. The transport equations are solved quantum mechanically under the non-equilibrium Green's function (NEGF) formalism and relies on a single-band effective mass Hamiltonian. The treatment of electron phonon scattering is done under the self consistent Born approximation (SCBA). We investigate in detail the effect of different acoustic and optical phonon modes on the drain current of the device for different channel lengths. We show that optical phonon mode with a deformation potential constant of 8.07×10^{8} eV/cm and energy $0.0421\,\mathrm{eV}$ plays the most important role in electron phonon scattering and subsequent degradation of ON current in devices along both directions. We also find that effect of electron phonon scattering is more pronounced along zigzag direction.**

***Keywords*-Phosphorene, dissipative transport, Non-Equilibrium Green's Function (NEGF) formalism, Self consistent Born approximation**

I. Introduction

Over the past few years, the field of semiconductor science and technology has witnessed extensive research on atomically thin two dimensional (2D) layered materials. The properties of these materials as well as their potential applications for transistor technologies are being studied both experimentally and theoretically. Most of these 2D materials *e.g.* hBN, Phosphorene, transition metal di-chalcogenides (TMD), such as MoS_2, WS_2, $MoSe_2$, WSe_2, $MoTe_2$ [1]–[6] are being extensively explored as an alternative channel material for metal oxide semiconductor field effect transistor (MOSFET), in order to meet the Moore's law projections.

Among these, Phosphorene a single atomic layer of Black Phosphorus with a puckered honeycomb lattice structure [4], [5], created a renewed interest among the researchers due to its high carrier mobility and highly anisotropic transport properties. Not only has it been theoretically investigated but also used in successful fabrication of transistors [4], [5], [7]–[10], [13]. Among the various theoretical reports [11]–[15] on performance projections of MOSFETs based on monolayer TMDs and Phosphorene, it is shown that Phosphorene MOSFETs outperform the TMD based MOSFETs in terms of ON current requirements and subthreshold swing characteristics. The noteworthy performance of Phosphorene MOSFETs is attributed to its very low effective mass along the armchair direction and moderate band gap.

Technology limitations compel most devices to act in the diffusive regime and this emphasizes the importance of incorporating electron phonon scattering for simulating realistic devices. This understanding will overall be useful to design high performance transistors using 2D materials. Most of the theoretical studies on Phosphorene FETs have been limited to ballistic transport. Only a couple of papers have reported the performance of Phosphorene MOSFET under electron-phonon scattering [14], [15]. However, the channel length considered in their studies is equal to $10\,\mathrm{nm}$ which is quite close to the ballistic limit and the detrimental effect of phonon scattering on the performance of MOSFET fades out at such shorter length devices. At the same time the effect of individual phonon modes on transport is not investigated. As a result, it is necessary to consider longer channel Phosphorene MOSFET to study accurately the effect of electron-phonon scattering on device performance. This motivated us to calculate the dissipative transport in Phosphorene MOSFET with a longer channel length of $20\,\mathrm{nm}$. Moreover, we investigate the effect of individual phonon branches on the ON current of the device, in order to estimate the phonon mode dominant for scattering in diffusive limit. In this work we use non-equilibrium Green's function (NEGF) equations under the self-consistent Born approximation (SCBA) to calculate the dissipative transport in n-type Phosphorene MOSFETs in both armchair and zigzag directions. We choose both directions because of the highly anisotropic property of effective masses in Phosphorene.

The paper is organized as follows. In Section II we describe the simulation methodology. In Section III we present and discuss our results by pointing out the effect of different electron-phonon interaction on the device transfer characteristics. Finally, in Section IV we draw our concluding remarks.

II. Methodology

Fig. 1 shows a schematic of the device cross-section under consideration. The effective oxide thickness (EOT) is $0.41\,\mathrm{nm}$, and supply bias $V_\mathrm{D} = 0.64\,\mathrm{V}$, chosen according to the ITRS 2013 specifications [16]. The length L_CH of the undoped channel is the same as the gate length L_G which is $20\,\mathrm{nm}$. The $15\,\mathrm{nm}$ long source and drain extensions are uniformly doped at $3\times10^{13}/\mathrm{cm}^2$ in order to satisfy charge neutrality conditions at the contact. The thickness of the Phosphorene layer is taken

2380-6923/19/$31.00 ©2019 IEEE
DOI 10.1109/VLSID.2019.00050

to be $0.6\,\mathrm{nm}$, as extracted from the atomic configuration used in density functional theory (DFT) calculations. The OFF-state current (I_{OFF}) at zero gate voltage (V_{G}) is set at $100\,\mathrm{nA/\mu m}$ by choosing an appropriate gate work function.

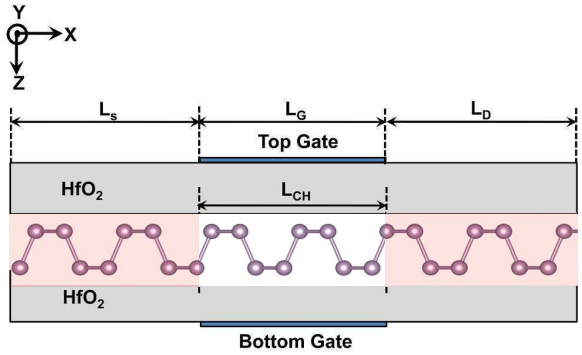

Fig. 1: Sketch of the cross-section of the considered Phosphorene MOSFET. L_{CH} denotes the channel length, which is set equal to the gate length L_{G}. The channel is undoped, while the source and drain extensions (shaded) are uniformly doped.

Firstly, we conduct DFT calculations to evaluate the carrier effective mass and the band gap. The DFT calculations are carried out using generalised gradient approximation (GGA) as implemented in the code VASP [17]–[19] with PAW [20] method using the Heyd-Scuseria-Ernzerhof (HSE) [21] hybrid functional in order to determine the electronic properties. $3s^2$ $3p^3$ electrons of Phosphorus are treated as valence electrons and expanded in plane wave basis set. A cutoff energy of $400\mathrm{eV}$ is used and a Γ-centered $15 \times 13 \times 1$ (in X, Y and Z directions) k-mesh is found suitable for sampling the Brillouin zone for structural relaxations whereas a denser k-mesh of $33 \times 29 \times 1$ is used for static calculations. Electronic convergence is achieved when the difference in energy of successive electronic steps becomes less than $10^{-6}\mathrm{eV}$, whereas the structural geometry is optimised until the maximum force on every atom falls below $0.01\mathrm{eV}/\mathring{A}$. A large vacuum space of more than $20\mathring{A}$ is applied in Z direction to avoid any interaction between successive layers. The phonon calculations are done using the code Phonopy [22] which uses atomic forces calculated by VASP using density functional perturbation theory (DFPT) on a 2×2 Phosphorene cell using a $27 \times 25 \times 1$ k-mesh.

The effective masses along armchair and zigzag directions are $0.171m_0$ and $1.104m_0$, respectively, m_0 being the free electron mass and band gap $1.603\,\mathrm{eV}$ as extracted from the DFT simulations. The following transport calculations are based on a single band effective mass hamiltonian using these material parameters.

Fig. 2 shows the phonon spectrum of Phosphorene generated from DFT calculations. The different modes are numbered as reported in [23]. Phonon modes 2 and 3 stand for the acoustic branches whereas 7, 9 and 11 stand for the optical branches. We also note down the corresponding deformation potential

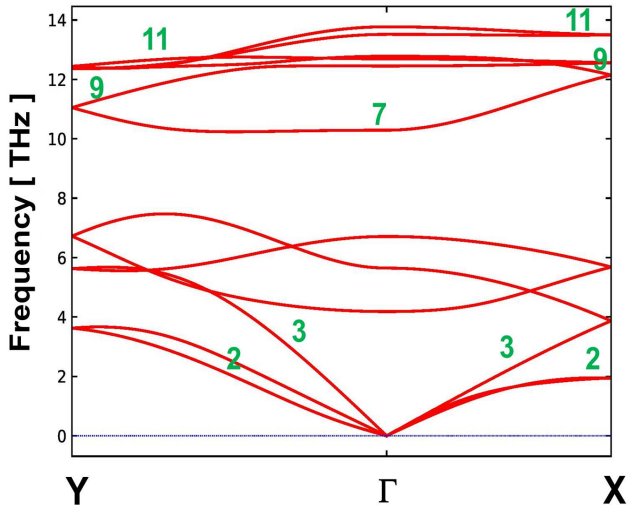

Fig. 2: Phonon dispersion of Phosphorene obtained from VASP. The different phonon branches considered in our simulation are marked. Branches 2 and 3 are acoustic phonons while the remaining marked branches stand for different optical modes [23]. It should be noted that between the two acoustic modes, phonon branch 3 has minimal effect compared to acoustic phonon branch 2 when transport is in armchair direction, whereas transport in zigzag direction is dominated by phonon branch 3 [23].

values and the frequencies of the optical phonon branches in Table I as reported in [23].

For calculating transport we solve the NEGF equations self-consistently with the Poisson's equation. Our assumption of translational invariance in the y direction of the device, enables to parametrize the Hamiltonian and the Green's functions in terms of the in-plane transversal wave vector k_y. Therefore, we can restrict the solution of the Poisson's equation to a cross-section in the x-z plane. We impose the Born-von Karman periodic boundary conditions in a system with finite length $L_y = 80\,\mathrm{nm}$ by including 20 uniformly spaced transversal wave vectors $k_{y,n} = 2\pi n/L_y$. For each wave vector k_y, the retarded Green's function (expressed in the matrix notation) is calculated as [24], [25]

$$G^{\mathrm{r}}(k_y, E) = [EI - H(k_y) - \Sigma^{\mathrm{r}}{}_{\mathrm{S}} - \Sigma^{\mathrm{r}}{}_{\mathrm{D}} - \Sigma^{\mathrm{r}}{}_{\mathrm{ph}}]^{-1} \qquad (1)$$

where E is the energy, $H(k_y)$ is the Hamiltonian matrix discretized along the transport direction x, I is the identity matrix and $\Sigma^{\mathrm{r}}_{\mathrm{S}}/\Sigma^{\mathrm{r}}_{\mathrm{D}}$ are retarded self-energy matrices associated to the source/drain contacts [24] and $\Sigma^{\mathrm{r}}_{\mathrm{ph}}$ is the retarded self energy matrix due to electron-phonon interaction. The retarded Green's function $G^{\mathrm{r}}(k_y, E)$ results in the calculation of the electron Green's functions $G^{<}(k_y, E)$ as follows:

$$G^{<}(k_y, E) = G^{\mathrm{r}}(k_y, E)\Sigma^{<}G^{\mathrm{r}\dagger}(k_y, E) \qquad (2)$$

TABLE I: Values of deformation potentials D (in unit 10^8 eV /cm for optical and in eV for acoustic) and phonon energies E_{ph} (in meV) for the various marked branches in the phonon spectrum [23]

Parameter	Acoustic		Optical		
	2	3	7	9	11
D	2.74	8.31	8.07	6.6	6.6
E_{ph}	-	-	42.1	51.9	55.0

where

$$\Sigma^{<} \equiv (\Sigma^{\text{r}} - \Sigma^{\text{r}\dagger}) \cdot f_{\text{S/D}} \tag{3}$$

with † denoting the transpose conjugate and $f_{\text{S/D}}$ denoting the Fermi-Dirac distribution function at source/drain. The dissipative transport is treated under the self consistent Born approximation (SCBA) where the scattering self energy is a functional of the Green's function. The self energy due to elastic scattering by acoustic phonons is formulated as [30]

$$\Sigma^{<}_{\text{ph(ac)}} \equiv M^2_{\text{ac}} G^{<}(i, E) \tag{4}$$

and of inelastic scattering by optical phonons is [30]

$$\Sigma^{<}_{\text{ph(op)}} \equiv M^2_{\text{op}} (N_B + \frac{1}{2} \pm \frac{1}{2}) G^{<}(i, E \pm \hbar\omega) \tag{5}$$

with

$$\begin{aligned} M^2_{\text{ac}} &= \frac{D^2_{\text{ac}} k_B T}{\rho V {v_{\text{p}}}^2} \\ M^2_{\text{op}} &= \frac{D^2_{\text{op}} \hbar^2}{2\rho V E_{\text{ph}}} \end{aligned} \tag{6}$$

where M^2_{ac} and M^2_{op} denote the coupling constants for acoustic and optical phonons, ω is the optical phonon frequency, N_B stands for the Bose distribution, i denotes the position index of discretised lattice points, D_{ac} and D_{op} are deformation potential constants, V is the mesh volume, ρ is the density per volume unit, v_{p} is the sound velocity and E_{ph} denotes the optical phonon energy. In (5) the '+' and '−' stand for phonon emission and absorption respectively. The interdependence between the equations of scattering self energies and the Green's function, demand for an iterative solution (see Fig. 3) until convergence is reached by preserving the conservation laws.

This additional iterative loop makes the computation expensive compared to ballistic approximation. The carrier and current density are calculated by the recursive Green's function algorithm [26], [27]. The recursive Green's function algorithm [29] is implemented using Mixed C and MATLAB [28] programming style to accelerate the computation. The transverse modes have been computed in parallel across different processor cores, thereby resulting in further reduction of computational time. The 2D Poisson's equation is discretised in the cross-section of the device by using finite volume method, enforcing Dirichlet boundary conditions at the metal gate electrodes and Neumann boundary conditions on the rest of the edges. The NEGF transport equations and the Poisson's equation are solved iteratively until self-consistency is achieved.

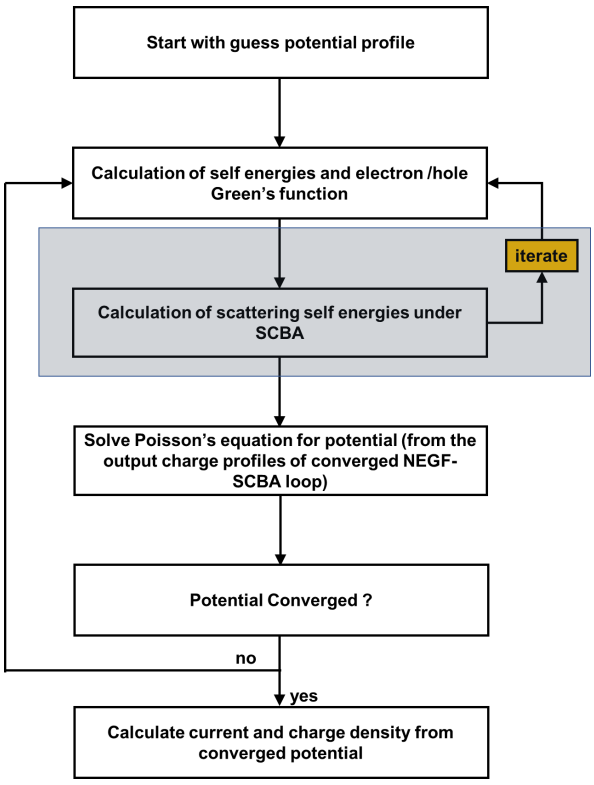

Fig. 3: Flowchart of dissipative quantum transport calculation. It should be noted that for ballistic transport the shaded block is omitted, but necessary only when we consider dissipative transport. The first two blocks are intertwined and run iteratively until the charge and current are conserved throughout the device. The first step starts off with a guess potential and the material hamiltonian as input. The input to the Poisson's equation are the device geometry and charge densities calculated from the electron and hole Green's function .

III. Results and Discussions

Fig. 4 shows the transfer characteristics of Phosphorene n-MOSFETs for both armchair and zigzag directions. The I_{D}-V_{G} curves are plotted for ballistic transport as well as for different electron-phonon interactions. From Fig. 4(a) and (b), we find that elastic acoustic phonon scattering plays an important role for low V_{G} but has an insignificant effect on the degradation of ON current. On the other hand, inelastic optical phonon scattering plays a dominant role at high V_{G} in degradation of

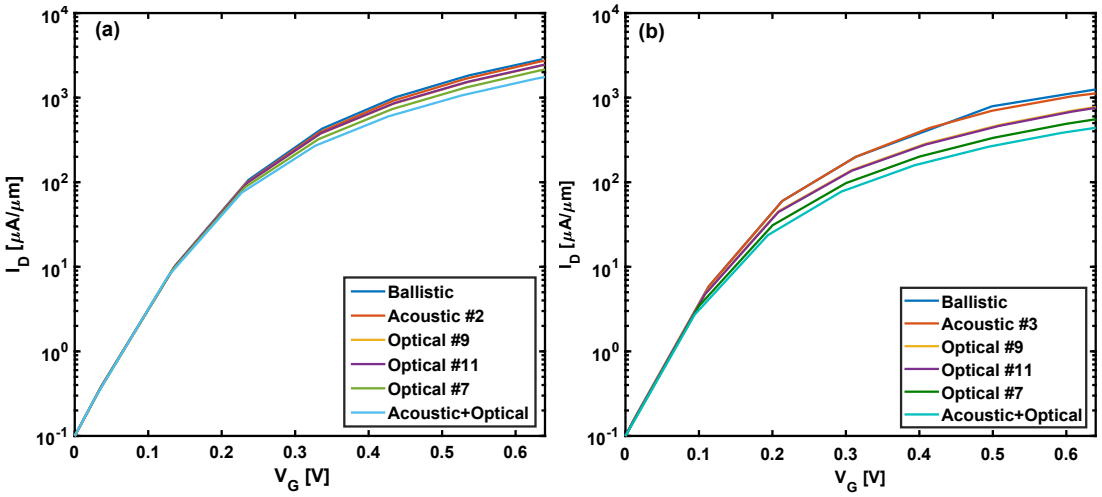

Fig. 4: Simulated transfer characteristics of Phosphorene n-MOSFETs for L_{CH} =20 nm when transport direction is (a) armchair and (b) zigzag.

ON state characteristics for both armchair and zigzag directions. Moreover, if we carefully examine the figure, we find that among all the optical phonon modes, the ON state current is affected mostly due to the interaction between electron and phonon mode 7 in both directions of transport. Our results follow the findings reported in [23] where it is found that the optical phonon branch 7 has the highest contribution to the scattering rate of electrons in the conduction band. The reason behind this phenomenon lies in the fact that optical phonon branch 7 has the highest deformation potential value and the lowest phonon energy (see Table I) which leads to increased backscattering of carriers by both emission and absorption. On the other hand, the remaining optical modes at higher phonon energy and a smaller deformation potential can backscatter through only emission resulting in a lesser amount of current loss.

Further, we note that the effect of scattering is stronger in case of Phosphorene MOSFETs along the zigzag directions. The reason is explained as follows. Due to a higher effective mass and consequently higher density of states, the potential barrier height is lower in case of zigzag MOSFET for the same current value as in armchair MOSFET. As a result, the effect of optical phonon backscattering becomes more pronounced in case of Phosphorene n-MOSFET along zigzag directions [32].

Next, we investigate the effect of electron-phonon interaction in shorter channel device (L_{CH} =10 nm). Fig. 5 shows the comparison between I_{D}-V_{G} plots of both 10 and 20 nm channels under ballistic and dissipative transport in linear as well as logarithmic scale. We notice that the effect of scattering diminishes in shorter channel length device and this reduces the decrease in ON current. This is further clear from the energy resolved current spectrum and velocity versus channel length plots of both the devices as shown in Fig. 6 and Fig. 7. As seen in the current spectrum plots,

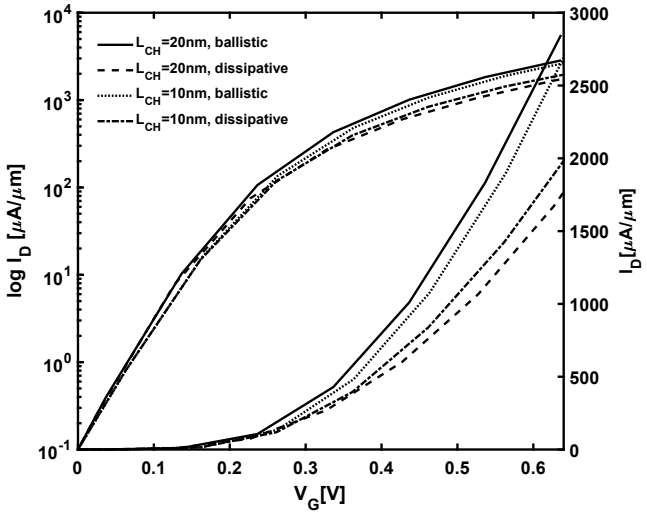

Fig. 5: Simulated transfer characteristics of Phosphorene n-MOSFETs for channel lengths of 10 and 20 nm along armchair direction under both ballistic and dissipative regime.

the inelastic emission process is stronger in case of longer channel Phosphorene n-MOSFET. This translates to a decrease in the carrier velocity (see Fig. 7) with respect to shorter channel device, and subsequent space charge accumulation at the source end which leads to considerable modulation of the channel potential in 20 nm device (see Fig. 7 (a) inset). This enhances the scattering and current loss mechanism [31]. However, in 10 nm devices, the carrier velocity is hardly affected by the inelastic emission process and this is reflected in the negligible change in the potential profile (see Fig. 7 (b) inset). Therefore, the degradation of ON current is minimal in ultra-scaled device, thereby enabling it to reach the ballistic

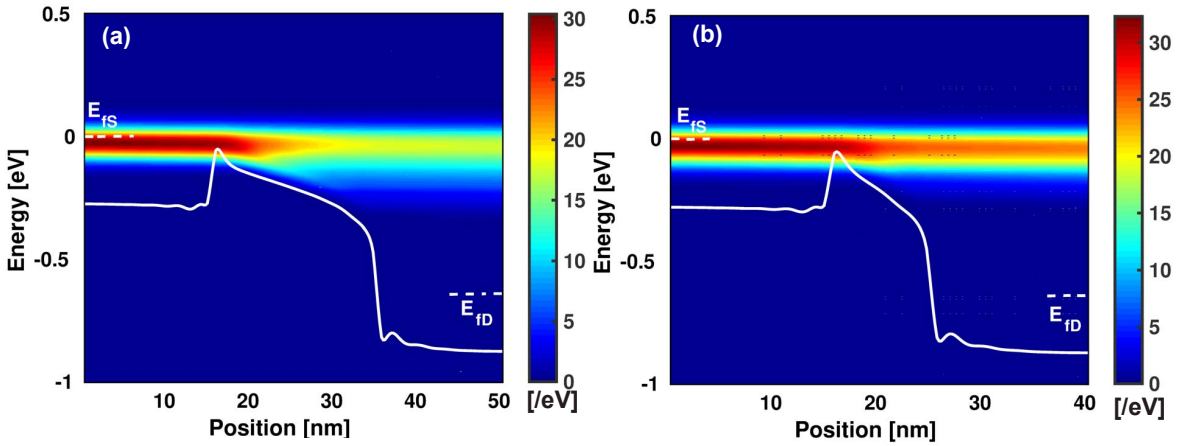

Fig. 6: Energy resolved current spectrum superimposed on the conduction band edge profile for Phosphorene n-MOSFET along armchair direction when (a) L_{CH} =20 nm and (b) L_{CH} =10 nm at ON-state *i.e.* $V_{\mathrm{D}} = 0.64\,\mathrm{V}$ and $V_{\mathrm{G}} = 0.64\,\mathrm{V}$.

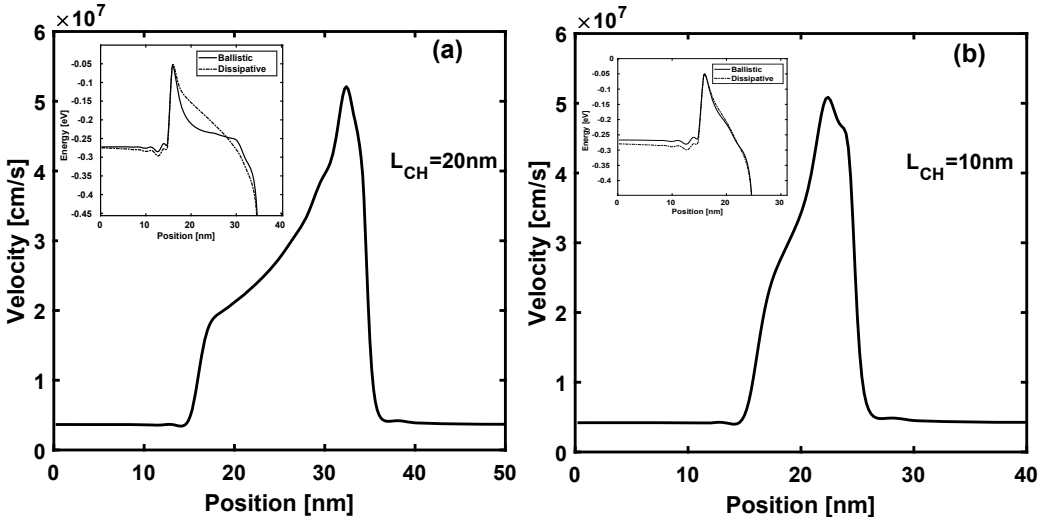

Fig. 7: Carrier drift velocity across the device length for (a) L_{CH} =20 nm and (b) L_{CH} =10 nm at ON-state *i.e.* $V_{\mathrm{D}} = 0.64\,\mathrm{V}$ and $V_{\mathrm{G}} = 0.64\,\mathrm{V}$. In the insets we compare the potential energy modulation inside the channel between ballistic and dissipative transport for both channel lengths.

limit. This observation further corroborates the fact that the study of diffusive transport in Phosphorene MOSFETs with 10 nm channel as reported in [14], is not suitable to accurately estimate the effect of scattering on Phosphorene MOSFETs, due to their near ballistic performance at such short channel lengths.

IV. Conclusion

We investigate through self consistent NEGF-SCBA equations the effect of different types of electron phonon coupling on the transfer characteristics of Phosphorene n-MOSFET along both armchair and zigzag directions. We find that zero order optical phonon mode having the highest deformation potential constant and the lowest energy, renders the strongest effect on the cumulative scattering rate in the devices thereby leading to degradation in ON current. We also note that the effect of scattering is more pronounced in transport along the zigzag direction as compared to armchair direction. Further we see that the effect of electron phonon scattering diminishes as the channel length is scaled down, thus pushing the device towards the ballistic limit.

Acknowledgment

The authors would like to thank Dr. Marc Bescond for helpful discussions.

REFERENCES

[1] B. Radisavljevic, M. B. Whitwick, and A. Kis, "*Integrated circuits and logic operations based on single-layer MoS_2*," ACS nano, vol. 5, no. 12, pp. 9934–9938, Nov. 2011, doi: 10.1021/nn203715c.

[2] S. B. Desai, S. R. Madhvapathy, A. B. Sachid, J. P. Llinas, Q. Wang, G. H. Ahn, G. Pitner, M. J. Kim, J. Bokor, C. Hu, and H. S. Wong, "*MoS2 transistors with 1-nanometer gate lengths*," Science, vol. 354, no. 6308 , pp. 99–102, Oct. 2016, doi: 10.1126/science.aah4698.

[3] H. Fang, S. Chuang, T. C. Chang, K. Takei, T. Takahashi, and A. Javey, "*High-performance single layered WSe_2 p-FETs with chemically doped contacts*," Nano Lett., vol. 12, no. 7, pp. 3788-–3792, Jun. 2012, doi: 10.1021/nl301702r.

[4] L. Li, Y. Yu, G. J. Ye, Q. Ge, X. Ou, H. Wu, D. Feng, X. H. Chen and Y. Zhang, "*Black Phosphorus Field Effect Transistors*," Nature nanotech., vol. 9, no. 5, pp. 372—377, Mar. 2014, doi: 10.1038/nnano.2014.35.

[5] H. Liu, A. T. Neal, Z. Zhu, Z. Luo, X. Xu, D. Tomanek and D. Y. Peide, "*Phosphorene: An Unexplored 2D Semiconductor with a High Hole Mobility*," ACS nano., vol. 8, no. 4, pp. 4033—4041, Mar. 2014, doi: 10.1021/nn501226z.

[6] K. S. Novoselov, D. Jiang, F. Schedin, T. J. Booth, V. V. Khotkevich, S. V. Morozov, and A. K. Geim, "*Two-dimensional atomic crystals*," Proc. Natl. Acad. Sci. U.S.A, vol. 102, no. 30, pp. 10451-–10453, Jul. 2005, doi: 10.1073/pnas.0502848102.

[7] W. Lu, H. Nan, J. Hong, Y. Chen, C. Zhu, Z. Liang, X. Ma, Z. Ni, Z, C. Jin and Z. Zhang, "*Plasma-assisted fabrication of monolayer phosphorene and its Raman characterization*," Nano Res., vol. 7, no. 6, pp. 853–859, May 2014, doi: 10.1007/s12274-014-0446-7.

[8] Z. Guo, H. Zhang,S. Lu, Z. Wang, S. Tang, J. Shao, Z. Sun, H. Xie, H. Wang, X. F. Yu and P . K. Chu, "*From black phosphorus to phosphorene: basic solvent exfoliation, evolution of Raman scattering, and applications to ultrafast photonics*," Adv. Funct. Mater., vol. 25, no. 45, Dec. 2015, pp. 6996–7002, doi: 10.1002/adfm.201502902

[9] L. Kou, C. Chen, S. C. Smith, "*Phosphorene: fabrication, properties, and applications*," J. Phys. Chem. Lett., vol. 6, no. 14, pp. 2794–805, Jun. 2015, doi:10.1021/acs.jpclett.5b01094.

[10] X. Luo, Y. Rahbarihagh, J. C. Hwang, H. Liu, Y. Du , D. Y. Peide, "*Temporal and thermal stability of Al_2O_3-passivated phosphorene MOSFETs*," IEEE Elec. Dev. Lett., vol. 35, no. 12, pp. 1314–1316, Dec. 2014. doi:10.1109/LED.2014.2362841.

[11] X. Cao, J. Guo, "*Simulation of phosphorene field-effect transistor at the scaling limit*," IEEE Trans. Elec. Dev., vol. 62, no. 2, pp. 659–665, Feb. 2015, doi: 10.1109/TED.2014.2377632.

[12] H. Ilatikhameneh, T. Ameen, B. Novakovic, Y. Tan, G. Klimeck, R. Rahman, X. Luo, Y. Rahbarihagh, J. C. Hwang, H. Liu, Y. Du , D. Y. Peide, "*Saving Moore's law down to 1 nm channels with anisotropic effective mass*," Sci. rep., vol. 6, no. 31501, Aug. 2016, doi: 10.1038/srep31501.

[13] N. Haratipour, S. Namgung, S. H. Oh, S. J. Koester, "*Fundamental limits on the subthreshold slope in Schottky source/drain black phosphorus field-effect transistors*," ACS nano., vol. 10, no. 3, pp. 3791–3800, Mar. 2016, doi: 10.1021/acsnano.6b00482.

[14] A. Szabo, R. Rhyner, H. Carrillo-Nunez, M. Luisier, "*Phonon-limited performance of single-layer, single-gate black phosphorus n-and p-type field-effect transistors*," IEEE International Electron Devices Meeting (IEDM), pp. 12–1, Dec. 2015, doi: 10.1109/IEDM.2015.7409680.

[15] M. Luisier, A. Szabo, C. Stieger, C. Klinkert, S. Brück, A. Jain, L. Novotny, "*First-principles simulations of 2-D semiconductor devices: Mobility, IV characteristics, and contact resistance*," IEEE International Electron Devices Meeting (IEDM), pp. 5–4, Dec. 2016, doi: 10.1109/IEDM.2016.7838353.

[16] International Technology Roadmap for Semiconductors. [Online]. Available:http://www.itrs2.net/2013-itrs.html

[17] G. Kresse and J. Furthmuller Kresse, "*Software VASP, Vienna (1999)*," G. Kresse and J. Hafner, Phys. Rev. B, vol. 47, no. 1, pp. 558 , Jan. 1993, doi: 10.1103/PhysRevB.47.558.

[18] G. Kresse, and J. Furthmuller, "*Efficient iterative schemes for ab initio total-energy calculations using a plane-wave basis set*," Phys. Rev. B, vol. 54, no. 16, pp. 11169–11186, Oct. 1996, doi: 10.1103/PhysRevB.54.11169.

[19] G. Kresse, and J. Furthmuller, "*Efficiency of ab-initio total energy calculations for metals and semiconductors using a plane-wave basis set*," Comp. Mater. Sci. vol. 6, no. 1, pp. 15—50, Jul. 1996, doi: 10.1016/0927-0256(96)00008-0.

[20] G. Kresse, G. and D. Joubert, "*From ultrasoft pseudopotentials to the projector augmented-wave method*," Phys. Rev. B , vol. 59, no. 3, pp. 1758–1775, Jan. 1999, doi: 10.1103/PhysRevB.59.1758.

[21] J. Heyd, G. E. Scuseria and M. Ernzerhof, "*Hybrid functionals based on a screened Coulomb potential*," J. Chem. Phys, vol. 118, no. 18, pp. 8207-–8215, May 2003, doi: 10.1063/1.1564060.

[22] Atsushi Togo and Isao Tanaka, "*First principles phonon calculations in materials science*," Scripta Mater., vol. 108, pp. 1–5, Nov. 2015, doi: 10.1016/j.scriptamat.2015.07.021.

[23] M. Elahi, M. Pourfath, "*Ab initio effective deformation potentials of phosphorene and consistency checks*," J. Phys.: Condens. Matter, vol. 30, no. 22, pp. 225701, May 2018, doi: 10.1088/1361-648X/aabdf4.

[24] S. Datta, "*Quantum transport: atom to transistor*," Cambridge University Press, 2005, doi: 10.1017/CBO9781139164313.

[25] J. Guo, "*Carbon nanotube electronics: Modeling, physics, and applications*," Ph.D. dissertation, Dept. Elect. Eng., Purdue Univ., West Lafayette, IN, USA, Aug. 2004. [Online]. Available: https://nanohub.org/resources/1928.

[26] R. Lake, G. Klimeck, R. C. Bowen and D. Jovanovic, "*Single and multiband modeling of quantum electron transport through layered semiconductor devices*," J. Appl. Phys. , vol. 81, no. 12, pp. 7845—7869 , Jun. 1997, doi: 10.1063/1.365394.

[27] M. P. Anantram, M. S. Lundstrom, and D. E. Nikonov. "*Modeling of Nanoscale Devices*," Proc. IEEE, vol. 96, no. 9, pp. 1511–1550, Sep. 2008, doi: 10.1109/JPROC.2008.927355.

[28] MATLAB version 9.1.0.441655 (R2016b), Sep. 7, 2016.

[29] Z. Jiang, "*Quantum transport in RTD and atomistic modeling of nanostructures*," Masters dissertation, Dept. Elect. Eng., Purdue Univ., West Lafayette, IN, USA, 2011.

[30] M. Bescond, C. Li, H. Mera, N. Cavassilas, M. Lannoo, "*Modeling of phonon scattering in n-type nanowire transistors using one-shot analytic continuation technique*," J. Appl. Phys., vol. 114, no. 15, pp.153712(1)–(7), Oct. 2013, doi: 10.1063/1.4825226.

[31] H. Tsuchiya, S. I. Takagi, "*Influence of elastic and inelastic phonon scattering on the drive current of quasi-ballistic MOSFETs*," IEEE Trans. Elec. Dev., vol. 55, no. 9, pp. 2397–2402, Sep. 2008, doi: 10.1109/TED.2008.927384.

[32] S. O. Koswatta, S. Hasan, M. S. Lundstrom, M. P. Anantram, D. E. Nikonov, "*Non-equilibrium Green's function treatment of phonon scattering in carbon nanotube transistors* ,"IEEE Trans. Elec. Dev., vol. 54, no. 9, pp. 2339–2351, Sep. 2007, doi: 10.1109/TED.2007.902900.